

# THE EFFECTS OF SKIN-STIFFENER BONDING FLAWS SIZE ON THE POST-BUCKLING BEHAVIOR OF COMPOSITE PANELS

**Mariano Andrés Arbelo, marbelo@ita.br**

**Maurício Vicente Donadon, donadon@ita.br**

**Sérgio Frascino Müller de Almeida, sergio.frascino@gmail.com**

Instituto Tecnológico de Aeronáutica, CTA-ITA-IEM, Praça Marechal Eduardo Gomes 50, Vila das Acácias, São José dos Campos – SP, Brasil, CEP: 12.215-790

**Abstract.** Applications have increasingly been made in substituting conventional mechanical fasteners by adhesive joints, especially in the aircraft and aerospace industries, where weight is a predominant factor. The presence of flaws such as defects in the adhesive layer between the skin and the stiffener may greatly affect the structural behavior of composite panels. The load transfer from the adherent to the adhesive is expected to be different from the idealized joint. In addition, localized stress concentrations induced by irregular adhesive defects that may be found in practical engineering applications can further reduce the strength of the stiffened composite panels. Within this context, this work presents a numerical investigation on the effects of skin-stiffener bonding flaw size on the post-buckling behavior of composite panels. The proposed model takes into account material and geometrical non-linearities in order to predict the structural response up to the collapse of the structure. In order to model the damage in the composite panel, a Continuum Damage Mechanics failure Model at meso-scale is combined with a newly developed contact logic to predict skin-stiffener debonding. The analysis were carried out using ABAQUS FE code. Quasi-static simulations using dynamic relaxation were performed for four different specimens with initial skin/stiffener debonding lengths of 0, 10, 30 and 50 mm. The simulated panels were loaded under axial compression up to the collapse, observing the progressive skin/stiffener debonding as well as its effects on the global structural behavior of the panels.

**Keywords:** Composites Materials, Damage Model, Post-buckling, Finite Elements.

## 1 INTRODUCTION

Fiber-reinforced composite materials have seen increased used in the aerospace industry as a result of their high specific strength and stiffness, amongst other properties. Harris *et al* (2002) show how the developments in construction using composite materials are following the growth and expansion of the aviation industry, starting with the design of parts of minor structural requirements. The developments progressed with the replacement of parts with considerable importance to the aircraft, finally evolving to the replacement of items which are critical to the performance of the aircraft. However, the application of post-buckling design with composite structures has been limited, as current analysis tools are not capable of accurately represent the damage mechanisms that lead to structural collapse of composites in compression. The critical failure mechanisms for stiffened composite structures in compression are skin-stiffener debonding, which includes adhesive failure in secondary-bonded structures or delamination at the skin-stiffener interface in co-cured structures, and fibre fracture in the stiffeners. Matrix cracking is generally not considered to be critical to structural collapse, but can have important local effects, so it is also an important failure mode.

The post-buckling and damage behavior of composite stiffened panels have been widely discussed in the open literature (Zimmermann *et al*, 2006, Degenhardt *et al*, 2007, Orifici *et al*, 2008 a-b). Many works have focused on the development of numerical models capable of predicting the skin-stiffener debonding of composite structures in the post-buckling regime (Krueger and Minguet, 2005, Bisagni, 2006, Degenhardt *et al*, 2008, Mikulit *et al*, 2008, Orifici *et al*, 2008 c-d).

Recently a considerable effort has been dedicated towards the development of fast and reliable design procedures for buckling, post-buckling and collapse analysis of fiber composite stiffened panels through the COCOMAT and POSICOSS European projects (Degenhardt *et al*, 2006).

## 2 OBJECTIVES

The main goal of this paper is to present a numerical investigation on the effects of skin-stiffener bonding flaw size on the post-buckling behavior of composite panels subjected to compression loading. Variations in maximum load and stiffness of the specimens will be evaluated according to the length of the initial defect. The numerical results allow to define a maximum acceptable defect size for use in quality control during production of the stiffened panel. Likewise, a maximum skin/stiffener debonding length may be set to use during the inspection process in operation.

### 3 FINITE ELEMENT MODEL

Simulations were carried out using ABAQUS® FE code to estimate the post-buckling behavior of stiffened composite panels. The proposed model takes into account material and geometrical non-linearities in order to predict the structural response up to the collapse of the structure. In order to model damage in the composite panel a Continuum Damage Mechanics Failure Model at meso-scale is combined with a newly developed contact logic to predict skin-stiffener debonding. The simulated panels, with initial skin/stiffener debonding lengths of 0, 10, 30 and 50 mm, were loaded under axial compression up to the collapse, observing the progressive skin/stiffener debonding as well as its effects on the global structural behavior of the panels.

The finite element model used in this work is shown in Fig. 1. The model is composed of three main parts: a skin, a stiffener and the skin-stiffener interface. The geometry of the stiffened panel is shown in Fig. 2 (a) and a cross-sectional view is presented in Fig. 2 (b). The stacking sequences are shown in Tab. 1. The thickness adopted in the skin-stiffener interface ( $h$ ) is 0.02mm. The mechanical properties of the material used in this study are presented in Tab. 2, where  $E_i$  is the Young modulus,  $G_{ij}$  is the in-plane shear modulus,  $\mu_{ij}$  is the poisson ratio,  $S_{ij}^k$  is the material strength associated with the failure mode  $k$  in the local direction defined by the subscripts  $ij$  ( $k = t$  for failure in tension,  $k = c$  for failure in compression and  $i = j = 1$  and  $i = j = 2$  refer to the fiber and matrix directions, respectively and  $i \neq j$  refer to in-plane shear direction),  $G_{ij}^k$  is the intralaminar fracture toughnesses associated with the failure mode  $k$  in the local direction defined by the subscripts  $ij$ ,  $GS$  is the in-plane shear intralaminar fracture toughness,  $t$  is the thickness layer.  $G_{IC}$ ,  $G_{IIC}$  and  $G_{IIIC}$  are the interlaminar fracture toughnesses for mode I, II and III of delamination respectively.

The stacking sequence and the material properties were taken from a previous experimental work of Arbelo (2008).

In the cases studied with initial bonding flaws, the model considers a region without any interface between the panel and stiffener. Additionally, contact effects between the skin and the stiffener are considered in order to avoid interpenetration between the components.

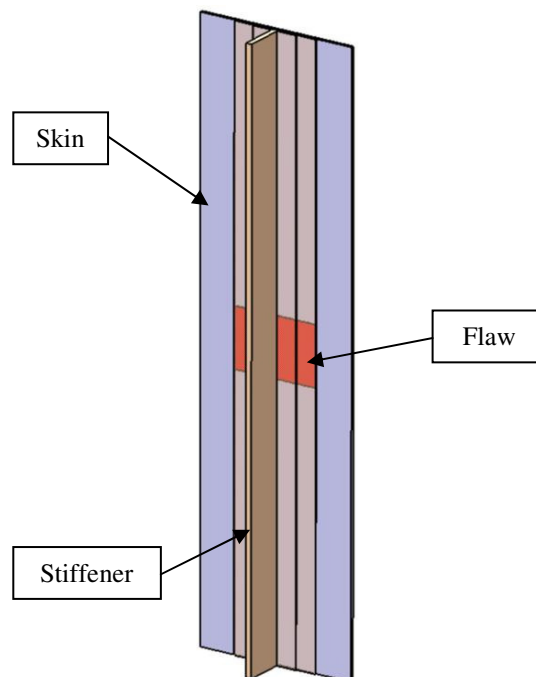


Figure 1. Finite element model.

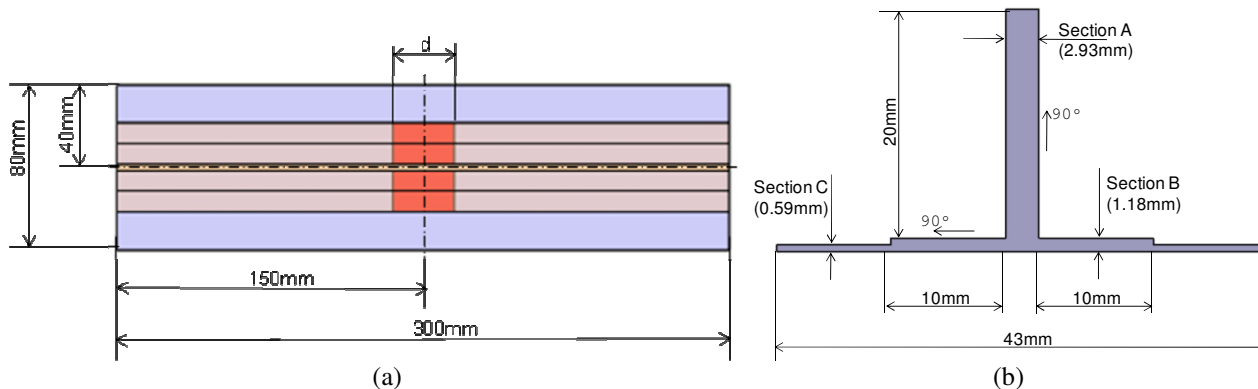


Figure 2. a) – b) Geometry of proposed stiffened panel (out of scale).

Table 1. Stacking sequence of proposed stiffened panel (Arbelo, 2008).

Section	Stacking sequence
Skin	$45^{\circ(F)}/0^{\circ(T)}_2/45^{\circ(F)}/0^{\circ(T)}_2/45^{\circ(F)}$
Section A	$45^{\circ(F)}/0^{\circ(T)}_2/45^{\circ(F)}/0^{\circ(T)}_7/45^{\circ(F)}/0^{\circ(T)}_2/45^{\circ(F)}$
Section B	$45^{\circ(F)}/0^{\circ(T)}_2/45^{\circ(F)}/0^{\circ(T)}_2$
Section C	$45^{\circ(F)}/0^{\circ(T)}_2$

(<sup>F</sup>): Fabric; (<sup>T</sup>): Tape

Table 2. Mechanical properties of materials (Arbelo, 2008).

Tape				
$E_1$ (GPa) = 125	$E_2$ (GPa) = 9.4	$G_{12}$ (GPa) = 4.7	$\mu_{12} = 0.32$	$S_{11}^T$ (MPa) = 1800
$S_{11}^C$ (MPa) = 1200	$S_{22}^T$ (MPa) = 30	$S_{22}^C$ (MPa) = 160	$G_{11}^T$ (kJ/m <sup>2</sup> ) = 160	$G_{11}^C$ (kJ/m <sup>2</sup> ) = 25
$G_{22}^T$ (kJ/m <sup>2</sup> ) = 10	$G_{22}^C$ (kJ/m <sup>2</sup> ) = 2,2	$S_{12}$ (MPa) = 105	$GS$ (kJ/m <sup>2</sup> ) = 2,2	$t$ (mm) = 0,19
Fabric				
$E_1$ (GPa) = 60	$E_2$ (GPa) = 58	$G_{12}$ (GPa) = 4.5	$\mu_{12} = 0.07$	$S_{11}^T$ (MPa) = 600
$S_{11}^C$ (MPa) = 750	$S_{22}^T$ (MPa) = 590	$S_{22}^C$ (MPa) = 700	$G_{11}^T$ (kJ/m <sup>2</sup> ) = 160	$G_{11}^C$ (kJ/m <sup>2</sup> ) = 25
$G_{22}^T$ (kJ/m <sup>2</sup> ) = 10	$G_{22}^C$ (kJ/m <sup>2</sup> ) = 2,2	$S_{12}$ (MPa) = 125	$GS$ (kJ/m <sup>2</sup> ) = 2,2	$t$ (mm) = 0,21
Interface				
$h$ (mm) = 0,02	$E_3$ (GPa) = 2,9	$G_{13}$ (GPa) = 1.08	$G_{23}$ (GPa) = 1.08	$S_{33}$ (MPa) = 50
$S_{13}$ (MPa) = 100	$S_{23}$ (MPa) = 100	$GI_C$ (kJ/m <sup>2</sup> ) = 0,58	$GII_C$ (kJ/m <sup>2</sup> ) = 3,5	$GIII_C$ (kJ/m <sup>2</sup> ) = 3,5

#### 4 MESO-SCALE CONTINUUM DAMAGE MECHANICS MODEL FOR COMPOSITE MATERIALS

The formulation proposed to model progressive failure in composites is based on the smeared cracking approach and has been extensively tested and validated in previous work (Donadon *et al* 2005, 2008, 2010, Yokoyama *et al* 2010, Arbelo *et al* 2010). The smeared cracking formulation relates the specific or volumetric energy, which is defined by the area underneath the stress-strain curve, with the strain-energy release rate of the material. The method assumes a strain softening constitutive law for modeling the gradual stiffness reduction due to the micro-cracking process within the cohesive or process zone of the material. In order to avoid pathological problem associated with strain localization and mesh dependence during softening, the softening portion of a stress-strain curve is adjusted according to the element topology and cracking direction for each failure mode using an advanced objectivity algorithm.

##### 4.1 Failure criteria

The failure criteria used to detect damage initiation for all in-plane failure modes are all based on the maximum stress criteria (tested and validated in previous work by Donadon *et al*, 2008; Yokoyama *et al*, 2010; and Arbelo *et al*, 2010) and they are given in the general form as follows:

$$F_{ij}^k(\sigma_{ij}) = \frac{\sigma_{ij}^k}{S_{ij}^k} - 1 \geq 0 \quad (1)$$

where  $F_{ij}^k(\sigma_{ij})$  is the failure index associated with the failure mode  $k$ , where  $k=t$  for failure in tension,  $k=c$  for failure in compression and  $k=s$  for failure in shear.  $\sigma_{ij}$  are the stresses acting on each layer at the local material coordinate system, where the subscripts  $i=j=1$  and  $i=j=2$  refer to the fiber and matrix directions, respectively and  $i \neq j$  refer to in-plane shear direction.  $S_{ij}^k$  is the material strength associated with the failure mode  $k$  in the local direction defined by the subscripts  $ij$ .

## 4.2 Damage evolution laws

### 4.2.1 Damage evolution law for fiber failure and matrix cracking

The general expression proposed for the damage evolution laws in the fiber and matrix directions is given as follows:

$$d_{ii}(\lambda_{i,1}, \lambda_{i,2}) = \lambda_{i,1} + \lambda_{i,2} - \lambda_{i,1} \lambda_{i,2} \quad (2)$$

with

$$\lambda_{i,1} = \frac{2G_{ii}^t}{2G_{ii}^t - S_{ii}^t l^* \epsilon_{i,0}^t} \left( \frac{\epsilon_{ii}^t - \epsilon_{i,0}^t}{\epsilon_{ii}^t} \right) \quad (3)$$

$$\lambda_{i,2} = \frac{2G_{ii}^c}{2G_{ii}^c - S_{ii}^c l^* \epsilon_{i,0}^c} \left( \frac{\epsilon_{ii}^c - \epsilon_{i,0}^c}{\epsilon_{ii}^c} \right) \quad (4)$$

where  $i$  assumes value equals to one for fiber failure and two for matrix cracking. The values for both functions  $\lambda_{i,1}, \lambda_{i,2} \in [0, 1]$ .  $G_{ii}^t$  and  $G_{ii}^c$  are the intralaminar fracture toughnesses in tension and compression, respectively.  $\epsilon_{i,0}^t$  and  $\epsilon_{i,0}^c$  are maximum strains prior to catastrophic failure in tension and compression, respectively. In order to account for damage irreversibility effects  $\epsilon_{ii}^k = \max \left[ \left| \epsilon_{ii}^{\max}(t) \right|, \epsilon_{i,0}^k \right]$  where  $\epsilon_{ii}^{\max}(t)$  is the maximum achieved strain in the strain versus time history. The superscript  $k$  refers to the fiber failure mode, that is,  $k=t$  for failure in tension and  $k=c$  for failure in compression. The characteristic length  $l^*$  is used for mapping the material process (or microcracking) zone into the finite element mesh. For fiber failure modes  $l^*$  is computed in terms of the isoparametric coordinates  $(\xi_m, \eta_m)$  for each integration point  $m$  according to the following expression,

$$l^*(\xi_m, \eta_m) = \left( \sum_{l=1}^{n_c} \left[ \frac{\partial N_l(\xi_m, \eta_m)}{\partial x} \cos(\theta_m) + \frac{\partial N_l(\xi_m, \eta_m)}{\partial y} \sin(\theta_m) \right] \phi_l \right)^{-1} \quad (5)$$

where  $\theta_m = \theta_{fibre}$  being  $\theta_{fibre}$  the fiber orientation angle for each integration point for fiber failure and  $\theta_m = \theta_{fibre} + 90^\circ$  for failure in the matrix direction. For a shell element with four nodes  $n_c = 4$ ,  $N_l(\xi_m, \eta_m)$  are bi-linear interpolation functions and  $\phi_l$  is defined as crack band discontinuity function. Details about the derivation of the expression for the characteristic length for orthotropic smeared cracking modes can be found in Donadon et al (2008).

### 4.2.2 Damage evolution law for in-plane shear failure

The damage evolution for in-plane shear failure is given by

$$d_{12}(\gamma_{12}) = \frac{\gamma_{12,f} \left[ 2(\gamma_{12} - \gamma_{12,0}^n) - \gamma_{12,f} \right]}{(\gamma_{12,f} + \gamma_{12,0}^n - \gamma_{12})(\gamma_{12} - \gamma_{12,0}^n)} \quad (6)$$

with

$$\gamma_{12,f} = \frac{2G_s}{S_{12} l^*} \quad (7)$$

where  $\gamma_{12,0}^n$  is the inelastic strain at failure and  $G_s$  is the in-plane shear intralaminar fracture toughness. The characteristic length  $l^*$  for in-plane shear failure is assumed to be the same as the one used for fiber failure modes.

### 4.3 Non-linear rate dependent in-plane shear model

The observed behavior of glass and carbon fiber laminates generally shows marked rate dependence in matrix dominated shear failure modes and for this reason a rate dependent constitutive model has been used to model the in-plane shear behavior. The constitutive model formulation is based on previous work carried out by Donadon and Iannucci (2006), and it accounts for shear non-linearities, irreversible strains and damage within the Representative Volume Element (RVE) of the material. The stress-strain behavior for in-plane shear failure is defined as follows:

$$\tau_{12} = \alpha G_{12} \gamma_{12} \quad (8)$$

with

$$G_{12} = G_{12}^0 + c_1 (e^{-c_2 \dot{\gamma}_{12}} - 1) \quad (9)$$

where  $G_{12}^0$  is the initial shear modulus and  $c_1$  and  $c_2$  are material constants obtained from in-plane shear tests.  $\alpha$  is the strain-rate enhancement given by the following law:

$$\alpha = 1 + e^{\frac{\dot{\gamma}_{12}}{c_3}} \quad (10)$$

where  $c_3$  is a material constant obtained from dynamic in-plane shear tests. By decomposing the total shear-strain into inelastic  $\gamma_{12}^m$  and  $\gamma_{12}^e$  elastic components, the inelastic shear strain can be written in terms of the elastic and total strain components as follows:

$$\gamma_{12}^m = \gamma_{12} - \gamma_{12}^e = \gamma_{12} - \frac{\tau_{12}(\gamma_{12})}{G_{12}^0} \quad (11)$$

### 4.4 Stress degradation procedure

The resultant degraded stresses at ply level are given by:

$$\begin{Bmatrix} \sigma_{11}^d \\ \sigma_{22}^d \\ \tau_{12}^d \end{Bmatrix} = \begin{bmatrix} (1-d_{11}(\lambda_1^f, \lambda_2^f)) & 0 & 0 \\ 0 & (1-d_{11}(\lambda_1^f, \lambda_2^f))(1-d_{22}(\lambda_1^m, \lambda_2^m)) & 0 \\ 0 & 0 & (1-d_{12}(\gamma_{12})) \end{bmatrix} \begin{Bmatrix} \sigma_{11} \\ \sigma_{22} \\ \tau_{12} \end{Bmatrix} \quad (12)$$

where

$$\begin{Bmatrix} \sigma_{11} \\ \sigma_{22} \\ \tau_{12} \end{Bmatrix} = \frac{1}{(1-\nu_{12}\nu_{21})} \begin{bmatrix} E_{11} & \nu_{12}E_{22} & 0 \\ \nu_{21}E_{11} & E_{22} & 0 \\ 0 & 0 & G_{12} \end{bmatrix} \begin{Bmatrix} \epsilon_{11} \\ \epsilon_{22} \\ \gamma_{12} \end{Bmatrix} \quad (13)$$

## 5 SKIN-STIFFENER DEBONDING CONTACT LOGIC

The contact logic is defined in terms of tractions and relative displacements between the upper and lower surfaces defining the interface. The relative displacement vector is composed of the resultant normal and sliding components defined by the relative movement between upper and lower surfaces of the contact element (see Fig. 3 (a)). The criteria for damage initiation and damage progression are given by Eq. (14) and (15), respectively. The constitutive law for a three dimensional stress case is shown in Fig. 3 (c).  $G_i$  is the strain-energy released rate defined by Eq. (16).  $K_{ii}$  is the interfacial stiffness in the direction  $ii$ , for  $i = I, II, III$ , and  $d$  is the damage parameter defined in Eq. (17). The mixed-mode delamination damage onset displacement vector is given in Eq. (18), and the final resultant displacement associated with the fully debonded interfacial behavior is given in Eq. (19).  $\alpha$ , and  $\beta$  are defined in Fig. 3 (b), and they are the angles that define the orientation of the resultant relative displacement vector. Details about the formulation are given in Donadon, et al (2009).

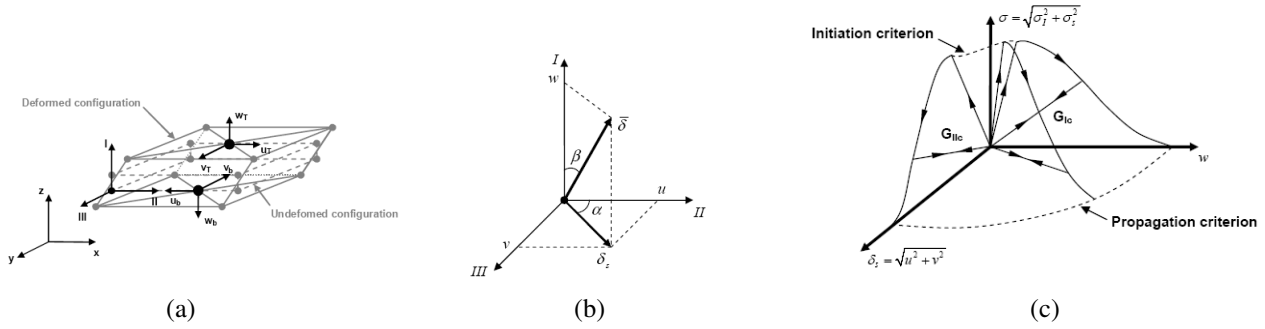


**Figure 3. Contact-logic: (a) 3D contact element, (b) Resultant displacement vector, (c) Constitutive law. (Donadon et al, 2009)**

$$\left(\frac{\sigma_I}{N}\right)^2 + \left(\frac{\sigma_{II}}{S_{II}}\right)^2 + \left(\frac{\sigma_{III}}{S_{III}}\right)^2 = 1 \quad (14)$$

$$\left(\frac{G_I}{G_{Ic}}\right)^\lambda + \left(\frac{G_{II}}{G_{IIc}}\right)^\lambda + \left(\frac{G_{III}}{G_{IIIc}}\right)^\lambda = 1 \quad (15)$$

$$G_i = \int_0^{\delta_i'} \sigma_i d\delta_i \rightarrow \sigma_i = K_{ii} (1-d) \delta_i \quad (16)$$

$$d = 1 - \frac{\bar{\delta}_0}{\bar{\delta}} \left[ 1 + \left( \frac{\bar{\delta} - \bar{\delta}_0}{\bar{\delta}_f - \bar{\delta}_0} \right)^2 \left( 2 \left( \frac{\bar{\delta} - \bar{\delta}_0}{\bar{\delta}_f - \bar{\delta}_0} \right) - 3 \right) \right] \text{ with } \bar{\delta} = \sqrt{u^2 + v^2 + w^2} \quad (17)$$

$$\bar{\delta}_0 = \left[ \left( \frac{K_{ww} \cos(\beta)}{N} \right)^2 + \left( \frac{K_{uu} \sin(\beta) \cos(\alpha)}{S_{II}} \right)^2 + \left( \frac{K_{vv} \sin(\beta) \sin(\alpha)}{S_{III}} \right)^2 \right]^{-1/2} \quad (18)$$

$$\bar{\delta}_f = \frac{2}{\bar{\delta}_0} \left[ \left( \frac{K_{ww} \cos(\beta)}{G_{Ic}} \right)^\lambda + \left( \frac{K_{uu} \sin(\beta) \cos(\alpha)}{G_{IIc}} \right)^\lambda + \left( \frac{K_{vv} \sin(\beta) \sin(\alpha)}{G_{IIIc}} \right)^\lambda \right]^{-1/\lambda} \quad (19)$$

## 6 POST-BUCKLING SIMULATION

### 6.1 Model Parameters

The finite element model was constructed using the ABAQUS software. Quasi-static simulations using dynamic relaxation were performed for four different specimens with initial skin/stiffener debonding lengths of 0, 10, 30 and 50 mm. The simulated panels were loaded under axial compression up to the collapse. A two-dimensional S4R element was used to model the skin and stiffener. The element has four nodes and it allows the definition of layers with different orientations through the thickness via user-defined integration rule. The modeling of the skin-stiffener interface was performed using the three-dimensional element C3D8R, which has eight nodes. Analysis of mesh sensitivity was performed for each configurations of the adopted initial imperfection, ensuring convergence of results in each case. The boundary conditions used for the analysis are presented in Fig. 4, where Tx, Ty and Tz represent the restriction of translation in the horizontal, vertical and out of plane axis respectively.

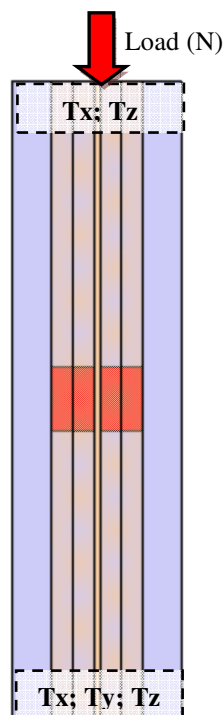


**Figure 4. Boundary conditions of finite element model.**

Table 3 shows the number of elements used in each model corresponding to the initial imperfection.

**Table 3. Number of elements used in each model.**

Model	Skin / Stiffener elements (S4R)	Interface elements (C3D8R)
d = 0	4320	1320
d = 10 mm	6048	1628
d = 30 mm	5544	1364
d = 50 mm	5832	1232

## 6.2 Results

Compression simulations were performed for stiffened panels with different levels of initial flaws. In the same way, a perfectly stiffened panel was also considered for comparison purposes. Figure 5 shows the results for compression load versus displacement. The solid circles present on the curves represent the initiation of the debonding propagation for each case. Table 4 shows, for each value of initial flaw, the maximum load and the decrease of load in percentage in models with initial imperfections compared to the perfect model.

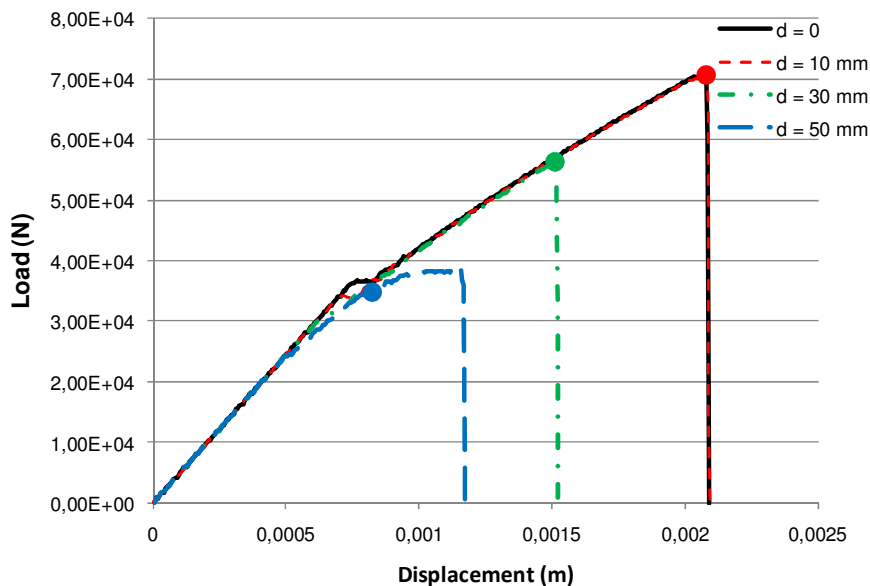


**Figure 5. Compression load versus displacement for each simulation.**

**Table 4. Ultimate compression load comparison.**

Model	Ultimate Load (N)	Decrease of maximum load (%)
d = 0	70982	0
d = 10 mm	70935	0.1
d = 30 mm	56458	20.5
d = 50 mm	39327	44.6

Some conclusions can be made by analyzing Fig. 5. For all simulated cases, the buckling of the stiffened panel occurs when the compressive load reaches approximately 35 kN. The compression load curve obtained from the model with an initial flaw of 10 mm is nearly equal when compared with the load curve of the perfect model. Moreover, for imperfection values of 30 and 50 mm, the local buckling of the stiffened panel begins to influence the general behavior of the structure, implying a reduction in the maximum load. It is also seen that for low values of imperfection, the initiation of debonding propagation between the panel and the stiffener coincides with the ultimate load of the component. For high values of initial flaws between the panel and the stiffener, the phenomenon of local buckling of the component is predominant in the debonded area. For these models, the debonding propagation between the skin and the stiffener occurs at constant load up to the catastrophic failure.

Similar results can be found in the work of Bisagni (2006) and Orifici *et al* (2008d). Experimental studies will be addressed in order to validate the finite element model.

## 7 CONCLUSION

A new methodology to modeling stiffened panels subjected to compressive load was presented and discussed in this work. The results show that the presence of imperfections in the skin-stiffener interface may cause a decrease in the ultimate load due to local buckling phenomena in the initial debonded area.

## 8 ACKNOWLEDGEMENTS

The authors acknowledge the financial support received from the Fundação de Amparo a Pesquisa do Estado de São Paulo (FAPESP), contract number 2008/05345-8 and CNPq Grants 305601/2007-5, 303287/2009-8.

## 9 REFERENCES

Arbelo, M. A., 2008, "Structural Behavior of Composite Laminated Panels Subjected to In-Plane Shear Loads", Master's Thesis (in Portuguese), Instituto Tecnológico de Aeronáutica.

- Arbelo, M. A., de Almeida, S. F. M., Donadon, M. V., 2010, "An experimental and numerical analysis for the post-buckling behavior of composite shear webs" *Composite Structures*, Vol. 93, No 2, pp. 465-473.
- Bisagni, C., 2006. "Progressive delamination analysis of stiffened composite panels in post-buckling". Proceedings of the 47 AIAA/ASME/ASCE/AHS/ASC Structures, Structural Dynamics, and Materials Conference. Rhode Island.
- Degenhardt R., Rolfes R., Zimmermann R., Rohwer K., 2006. "COCOMAT—improved material exploitation of composite airframe structures by accurate simulation of postbuckling and collapse", *Composite Structures*, Vol. 73, No 2, pp. 175-178.
- Degenhardt, R., Kling, A., Klein, H., Hillger, W., Goetting, H. C., Zimmermann, R., Rohwer, K., 2007, "Experiments on buckling and postbuckling of thin-walled CFRP structures using advanced measurement systems", *International Journal of Structural Stability and Dynamics*, Vol.7, No 2, pp. 337-358.
- Degenhardt, R., Kling, A., Rohwer, K., Orifici, A. C., Thomsson, R. S., 2008. "Design and analysis of stiffened composite panels including post-buckling and collapse", *Computers and Structures*, Vol. 86, pp. 919-929.
- Donadon, M.V., 2005 "The impact behavior of composite structures manufactured using resin infusion under flexible tooling", Ph.D Thesis, Department of Aeronautics, Imperial College London, England, UK, 375 p.
- Donadon, M. V. and Iannucci L., 2006 "Bird strike modeling using a new woven glass failure model", Proceedings of the LS-DYNA International Conference, Michigan, Dearborn, USA.
- Donadon, M.V., Iannucci,L., Falzon, B.G., Hodgkinson, J.M., de Almeida, S.F.M., 2008, "A progressive failure model for composite laminates subjected to low velocity damage", *Computers & Structures*, 86, pp.1232-1252.
- Donadon M.V., de Almeida S.F.M., Arbelo M. A., 2009, "A contact logic for mixed mode delamination modelling in composite laminates", to be published in an International Journal.
- Donadon, M.V., Arbelo, M.A., de Almeida, S.F.M., Actis, M., Pantanella, A.J., 2010, "Bird strike modeling in composites stiffened panels", Proceedings of 11th Pan-American Congress of Applied Mechanics", Foz do Iguaçu, Brazil.
- Harris C. E., Starnes Jr. J. H. and Shuart M. J., 2002."Design and Manufacturing of Aerospace Composite Structures - State-of-the-Art Assessment", *Journal of Aircraft*, Vol. 39, No 4, pp. 545-560.
- Krueger, R., Minguet, P. J., 2005. "Skin-Stiffener debond prediction based on computational fracture analysis", NASA/CR-2005-213915.
- Mikulik, Z., Kelly, D. W., Prusty, B. G., Thomson, R. S., 2008. "Prediction of flange debonding in composite stiffened panels using an analytical crack tip element-based methodology", *Composite Structures*, Vol. 85, pp. 233-244.
- Orifici, A. C., Abramovich, H., Herszberg, I., Kotler, A., Weller, T., Thomsson, R. S., Bayandor, J., 2008a, "Failure in skin-stiffener interfaces under post-buckling loads". Proceedings of the 2nd International Conference on Buckling and Postbuckling Behaviour of Composite Laminated Shell Structures.
- Orifici, A. C., Thomsson, R. S., Degenhardt, R., Kling, A., Rohwer, K., Bayandor, J., 2008b, "Degradation investigation in a postbuckling composite stiffened fuselage panel", *Composite Structure*, Vol. 82, pp. 217-224.
- Orifici, A. C., Thomson, R. S., Herszberg, I., Weller, T., Degenhardt, R., Bayandor, J., 2008c. "An analysis methodology for failure in postbuckling skin-stiffener interfaces". *Composite Structures*, Vol. 86, pp. 186-193.
- Orifici, A. C., Alberdi, I. O. Z., Thomson, R. S., Bayandor, J, 2008d. "Compression and post-buckling damage growth and collapse analysis of flat composite stiffened panels". *Composites Science and Technology*, Vol. 68, pp. 3150-3160.
- Yokoyama, N. O., Donadon, M.V., de Almeida, S.F.M., 2010, "A numerical study on the impact resistance of composite shells using an energy based failure model", *Computers & Structures*, 93, pp.142-152.
- Zimmermann, R., Klein, H., Kling, A., 2006. "Buckling and postbuckling of stringer stiffened fibre composite curved panels – Test and computations", *Composite Structures*, Vol. 73, pp. 150-161.

## 10 RESPONSIBILITY NOTICE

The authors are the only responsible for the printed material included in this paper.